RESEARCH ARTICLE SUMMARY

NEUROSCIENCE

Manipulating synthetic optogenetic odors reveals the coding logic of olfactory perception

Edmund Chong*, Monica Moroni*, Christopher Wilson, Shy Shoham, Stefano Panzeri, Dmitry Rinberg†

INTRODUCTION: Advances in monitoring brain activity at large and fine scales have revealed tremendous complexity in how the brain responds to, and represents, the external world. Although many features in brain activity patterns (which brain cells fire and when) are found to correlate with changes in the external sensory world, it is not yet known which activity features are consequential for perception and how they are combined to generate percepts. Some studies have shown that many of these correlated changes in activity may be redundant or even epiphenomenal.

RATIONALE: To address how brain activity generates perception, we directly and systematically manipulated neural activity in the mouse olfactory system while measuring perceptual responses. Mouse olfaction is an attractive model system because the relevant brain circuitry has already been carefully mapped out and is accessible for direct manipulation. We used genetically engineered mice in which brain cells can be activated simply by shining light on them—a technique known as optogenetics. Optogenetics allowed us to directly generate and manipulate brain activity in a precise and parametric manner. We first trained mice to recognize light-driven activity patterns in the olfactory system, or "synthetic odors." Subsequently, we measured how recognition changed as we systematically manipulated learned activity patterns. Some manipulations led to larger changes in recognition than others, and the degree of change reflected the importance of each manipulated feature to perception. By the additional manipulation of multiple features simultaneously, we could precisely quantify how individual features combined to produce perception.

A Mice were trained to recognize "synthetic odor" pattern

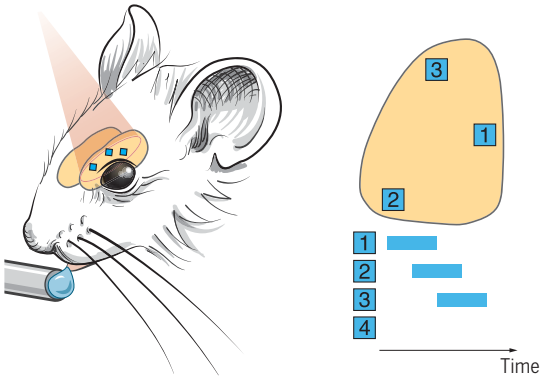

B Changes in recognition patterns were measured as trained pattern was modified

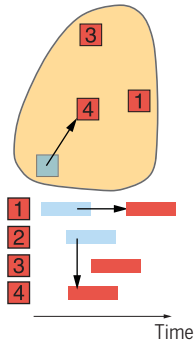

C Template matching model explains olfactory perception

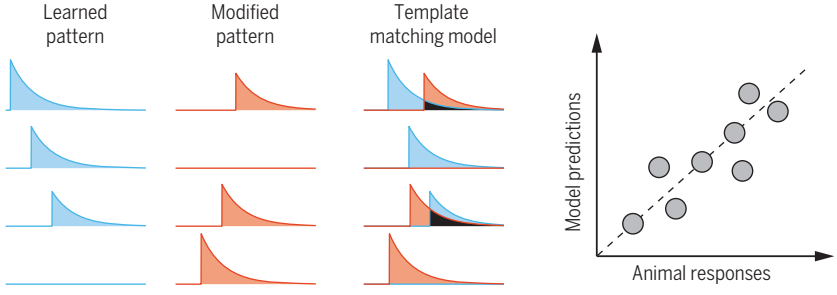

Probing olfactory perception with synthetic odors. (**A**) We trained mice to recognize synthetic odor patterns: artificially stimulated neural activity in the olfactory bulb. Patterns were defined in space (top right) and time (bottom right). (**B**) Perceptual responses were measured across systematic modifications of trained patterns. (**C**) Template-matching model of pattern activity (left) accounts for perceptual responses (right).

RESULTS: The perceptual responses of mice not only depended on which groups of cells were activated, but also on their activation latencies, i.e., temporal sequences akin to timed notes in a melody. Critically, the most perceptually relevant activation latencies were defined relative to other cells in a sequence and not to brain or body rhythms (e.g., animal sniffing) as previously hypothesized from observational studies. Moreover, earlier-activated cells in the sequence had a larger effect on behavioral responses; modifying later cells in the sequence had small effects. To account for all results, we formulated a simple computational model based on template matching, in which new activity sequences are compared with learned sequences or templates. The model weighs relative timing within each sequence and also accounts for the greater importance of earlier-activated cells. Based on our model, the degree of mismatch between the new sequence and learned template predicts the extent to which recognition should degrade as neural activity changes across many different manipulations.

ON OUR WEBSITE

Read the full article at https://dx.doi.org/10.1126/science.aba2357

CONCLUSION: We developed an experimental and theoretical framework to map a broad space of precisely and systematically manipulated brain activity patterns to behavioral responses. Using this framework, we uncovered key computations made by the olfactory system on neural activity to generate percepts and derived a systematic model of olfactory processing directly relevant for perception. Our framework forms a powerful, general approach for causally testing the links between brain activity and perception or behavior. This framework is especially pertinent given the continued development of advanced tools for manipulating brain activity at fine scales across various brain regions. ■

*These authors contributed equally to this work.
†Corresponding author. Email: rinberg@nyu.edu
The list of author affiliations is available in the full article online.
Cite this article as E. Chong *et al.*, *Science* **368**, eaba2357 (2020). DOI: 10.1126/science.aba2357

RESEARCH ARTICLE

NEUROSCIENCE

Manipulating synthetic optogenetic odors reveals the coding logic of olfactory perception

Edmund Chong[1]*, Monica Moroni[2,3]*, Christopher Wilson[1], Shy Shoham[1,4,5,6], Stefano Panzeri[2], Dmitry Rinberg[1,4]†

How does neural activity generate perception? Finding the combinations of spatial or temporal activity features (such as neuron identity or latency) that are consequential for perception remains challenging. We trained mice to recognize synthetic odors constructed from parametrically defined patterns of optogenetic activation, then measured perceptual changes during extensive and controlled perturbations across spatiotemporal dimensions. We modeled recognition as the matching of patterns to learned templates. The templates that best predicted recognition were sequences of spatially identified units, ordered by latencies relative to each other (with minimal effects of sniff). Within templates, individual units contributed additively, with larger contributions from earlier-activated units. Our synthetic approach reveals the fundamental logic of the olfactory code and provides a general framework for testing links between sensory activity and perception.

A familiar object evokes a complex pattern of activity in the brain. However, it is possible that only a structured subset of this activity, representing critical combinations of sensory attributes, is essential for recognition. A key challenge is to identify the essential components of neural activity that induce the percept. This activity may consist of multiple spatial or temporal features, such as which cells respond and when they respond relative to stimulus onset or each other. Do individual features contribute differentially to the formation of the percept? For example, the activity of some cells in a pattern may be more important than others. Does the formation of the percept depend on how features are combined? The sequential activation of multiple cells or the latency of their activation relative to brain rhythms are examples of feature combinations that may be perceptually meaningful (*1*–*3*).

The difficulty in addressing these questions is twofold. First, multiple features covary with perceptual responses, making it difficult to disentangle their independent contributions to perception. Previous studies have mainly focused on correlating neural activity with perception, in which the contributions of individual features are entangled. Although diverse stimulus sets may potentially disentangle feature contributions, biophysical constraints often impose strong correlations between features, which makes finding such stimulus sets difficult if not impossible. Second, we lack a single framework for quantitatively comparing the perceptual contributions of individual and combined features. For example, we know that single neurons (*4*) or small timing differences (*5*–*7*) can affect perception, but not their relative importance and how they come together in larger patterns to produce perception.

We investigated the link between neural activity and perception using olfaction as our model system. Odor perception is correlated with complex spatiotemporal activity patterns, and these patterns can be optogenetically manipulated in mice while measuring their perceptual responses. Odor-induced activity recruits glomeruli and spatiotemporal combinations of glomerular activity correspond to specific odorants (*8*, *9*). Both the spatial identity and temporal latencies of glomeruli activated in the pattern may be perceptually meaningful (*6*, *7*) but the relative importance of each is unknown. It is also unclear what forms a perceptually meaningful combination of glomerular activation: ordered sequences aligned relative to each other (*10*–*12*), sequences aligned to sniff rhythm (*6*, *7*, *13*, *14*), or the earliest activated subset of glomeruli within a sniff rhythm (*15*, *16*).

Here, we optogenetically manipulated individual activity features independently of other features, manipulated combinations of features, and compared the effects of all manipulations under a common metric.

Results

We first characterized the basic behavioral and neural responses to optogenetic stimulation. We chronically implanted OMP-ChR2-YFP mice ($n = 6$) (*6*) with cranial windows to expose the dorsal olfactory bulb and performed optogenetic stimulation (Fig. 1A). Similar to previous reports (*11*, *17*) and consistent with known anatomy, mitral tufted (MT) cells were activated by few localized spots (Fig. 1B and fig. S1, A and B). We observed instantaneous MT cell firing rates up to ~100 Hz, with excitatory responses lasting ~80 ms, comparable to odor-evoked responses (*13*). All spots at the same stimulation parameters were perceptually detectable but only for ChR2-positive mice (Fig. 1C) and without systematic spatial biases (Fig. 1D). We then used the same basic stimulation parameters for the main experiments.

We trained mice to discriminate Target versus Non-target synthetic odors on a two-choice task (Fig. 1E). Although the stimulation patterns we used are unlikely to correspond to specific known chemical odorants, our patterns follow stimulation durations and activation latencies that fall within known odor-evoked distributions of glomerular activation (*8*). Mice learned to discriminate a fixed Target from any random Non-target pattern over weeks, whereas ChR2-negative mice did not (Fig. 1F).

We then performed systematic spatial and/or temporal perturbations within Target patterns on a small number (10%) of probe trials and measured perceptual responses. Perturbations consisted of replacing spots with Non-target spots or shifting spots in time. For any set of perturbations, we measured the fraction of trials in which the mouse made a lick choice toward the water spout associated with the Target ("like-Target" response) as opposed to the Non-target spout. This measurement reflects perceptual distances (*18*, *19*): the perceived difference between the perturbed and original Target pattern. The larger the perceptual distance, the lower the fraction of like-Target responses. We performed a basic check to verify that perceptual distances increased as Target patterns were altered. In a pilot group of mice trained on the task, we systematically decreased the laser intensity below the intensity used during training. As the laser intensity for Target patterns was lowered, animals showed a graded decrease in like-Target responses (Fig. 1G).

Spatial perturbations led to graded changes in perceptual distances that were dependent on the timing of the spot perturbed. To perform spatial perturbations, we kept Target pattern timing fixed while replacing spots with random Non-target spots (Fig. 2A). One or more spots in the Target patterns were replaced in every possible combination of the six spot positions. We found a graded relationship between the number of spots replaced and perceptual distance (Fig. 2B). Spot replacement effects also depended on spot timing: Replacing earlier-activated spots had a greater effect than later-activated spots in both single-spot and multiple-spot replacement trials (Fig. 2C). We refer to this temporal

[1]Neuroscience Institute, NYU Langone Health, New York, NY 10016, USA. [2]Neural Computation Laboratory, Istituto Italiano di Tecnologia, 38068 Rovereto, Italy. [3]CIMeC, University of Trento, Rovereto, Italy. [4]Center for Neural Science, New York University, New York, NY 10003, USA. [5]Tech4Health Institute, NYU Langone Health, New York, NY 10010, USA. [6]Department of Ophthalmology, NYU Langone Health, New York, NY 10017, USA.
*These authors contributed equally to this work.
†Corresponding author. Email: rinberg@nyu.edu

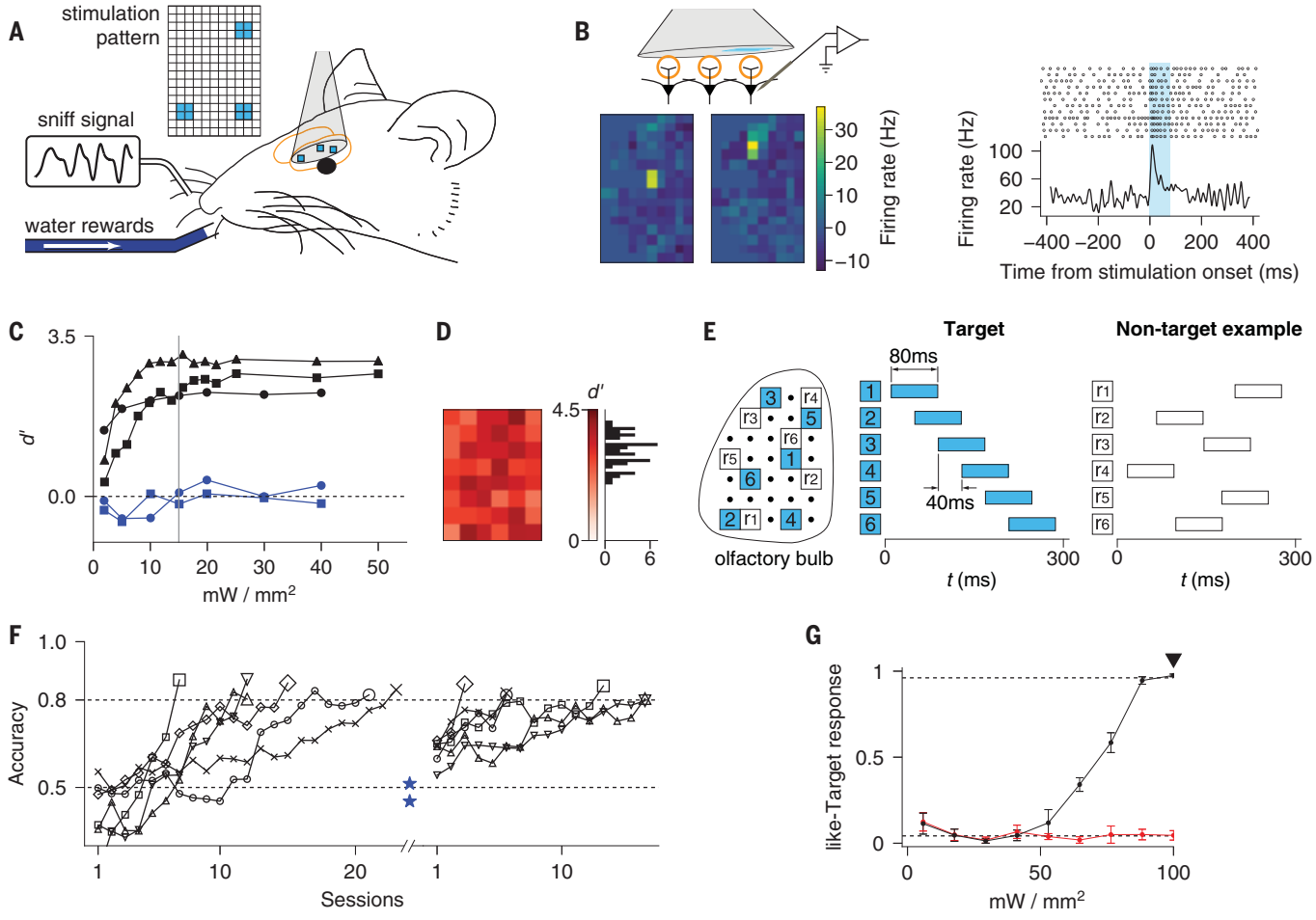

Fig. 1. Optogenetic stimulation as synthetic odors. (**A**) Schematic of the experimental setup. Dorsal olfactory bulb was exposed by a chronically implanted 3-mm window. Spatiotemporal stimulation patterns, created by a digital micromirror device, were projected onto the olfactory bulb of a head-fixed mouse in front of a pressure sensor for sniff monitoring, and lick spouts delivering water. (**B**) MT cell responses to single-spot stimulation (120 × 120 μm^2, 80-ms duration, 15 mW/mm^2) across a grid of spots. Left: Heatmaps of evoked firing (average firing rate across the stimulus duration, 80 ms) for each stimulated spot position for two typical cells. Right: Trial-by-trial spiking activity and peristimulus time histogram corresponding to left cell in (B) for the spot that evoked the largest averaged response. (**C**) Behavioral detection (d', or sensitivity index) of single-spot stimulation at different laser intensities for ChR2-positive animals (black) or ChR2-negative animals (blue). Gray vertical line marks 15 mW/mm^2. (**D**) Left: Heatmap of d' for spot detection at 15 mW/mm^2 stimulation for one ChR2 mouse at different spot positions. Right: Histogram of d' across spots. (**E**) Schematics for pattern discrimination task. Animals were trained to recognize Target versus Non-target patterns defined on a stimulation grid. Target patterns comprised six spots, initialized randomly but fixed across subsequent sessions, activated in an ordered sequence defined in time where 0 marks inhalation onset. Non-target patterns were six off-Target spots, randomly chosen from trial to trial, with randomized timing within 300 ms from inhalation (~single sniff). (**F**) Learning curves on pattern discrimination task. Mice were initially shaped by discriminating one Target pattern versus one Non-target pattern (left) to criterion performance of 0.8, then trained on the same Target versus multiple Non-target patterns (right). Note that performance below chance level (0.5) for some mice at the beginning of training is explained by a strong initial side bias (see the materials and methods). Blue stars indicate performance of control, ChR2-negative mice after >40 sessions of training. (**G**) Effect of reducing laser intensity on pattern recognition for mice previously trained to discriminate Target versus Non-target patterns at 100 mW/mm^2 (arrowhead). Shown is the probability of like-Target responses (mean ± SEM across mice) on probe trials with randomly chosen low-intensity Target patterns (black) and Non-target patterns (red). Horizontal dashed lines correspond to baseline responses to Target and Non-target patterns.

dependence as "primacy" (*15*). We additionally found that the effect of spot replacement depends on spatial distance on the olfactory bulb (fig. S2A). For these measurements, we used a larger dataset including other animals (fig. S3, A, C, and D). On average, the perceptual distance was larger between a Target and a Target with one spot replaced by a more distant spot. Because we did not measure spatial perturbations of Target locations at systematically defined locations across the olfactory bulb, our results reveal some chemotopy, but we cannot make conclusions about its characteristic length scale. Our effect was averaged across Target spot locations but could be location dependent. For example, if a Target spot was situated near to (far from) the boundary between odor receptor domains (*20*), replacing the spot with nearby spots would have large (small) effects. Our results are consistent with studies that suggest broad odor domains (*21*, *22*) and others that rule out fine-scale chemotopy (*23*–*25*). We also cannot completely rule out the alternative possibility that these effects may arise from activating fibers of passage, with strength of activation dependent on distance. However, these effects are likely to be weak: Mitral cell responses revealed only weak and spatially confined effects of fibers of passage (Fig. 1B and fig. S1), similar to other results using comparable stimulation parameters

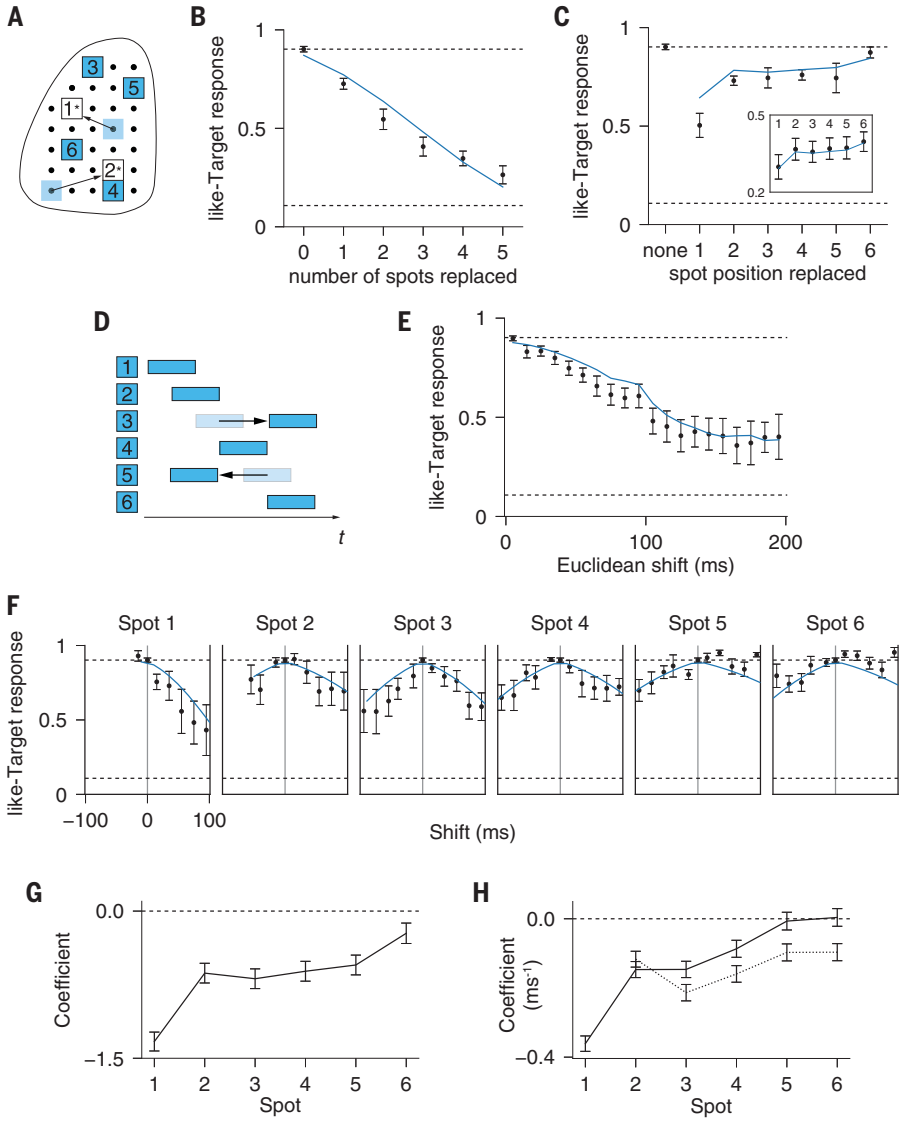

Fig. 2. Perceptual effects of spatial and temporal perturbations. (**A**) Illustration of spatial perturbations: One or multiple spots in Target patterns were randomly replaced with Non-target spots. (**B**) Probability of like-Target responses as a function of number of replaced spots in Target patterns averaged across animals. Here and later in plots of like-Target responses, horizontal dashed lines correspond to baseline responses to Target and Non-target patterns and blue lines show the corresponding regression fits. (**C**) Probability of like-Target responses as a function of a spot position for single-spot replacement. Inset: Probability of like-Target responses as a function of a spot position marginalized over trials with multiple spots replaced. (**D**) Illustration of temporal perturbations in which one or multiple spots in Target patterns were temporally shifted. (**E**) Probability of like-Target responses as a function of the amount of temporal shift ("Euclidean shift") in the pattern. (**F**) Effect of single-spot shifts plotted by spot position. (**G**) Regression coefficients showing the effect of replacing each spot in all trials, including single or multiple spot replacement. Negative coefficients imply that replacing the spot lowers like-Target responses; coefficients of zero imply no effect on responses. Regression coefficients represent the change in log-odds per unit change in the corresponding variable. (**H**) Same as (G) but for temporal perturbations. Separate coefficients were fitted for positive shifts (toward the end of the sniff cycle, solid line) and negative shifts (toward the beginning of the sniff cycle, dashed line).

(*11*). Furthermore, spatial replacement effects did not show any anisotropy that reflects the anatomy of passing fibers (fig. S2B).

Temporal perturbations also led to graded changes in perceptual distances dependent on the timing of the spot perturbed. To perform temporal perturbations, we shifted one or more spots of the Target pattern in 10-ms increments in randomly chosen combinations of spot and shift magnitude (Fig. 2D). Increasing the overall amount of temporal shift (defined as Euclidean shift = $\sqrt{\sum_i \Delta t_i^2}$ where Δt_i are individual spot shifts) led to an increase in perceptual distance (Fig. 2E). Similar to spatial perturbations, temporal perturbations also exhibited primacy. In trials in which only one spot was shifted, shifting earlier-activated spots had stronger effects than shifting later-activated spots (Fig. 2F). Furthermore, we observed an asymmetry in temporal shift effects: Shifting spots earlier, toward the beginning of the sniff cycle, had a stronger effect than shifting spots later, toward the end of the sniff cycle. This asymmetry is consistent with primacy: Although later-activated spots were less important perceptually, shifting them earlier may interfere with the early, more important spots, hence inducing larger behavioral effects.

To quantify the effect of spatial and temporal perturbations, we performed regression analyses using either binary variables for spot replacement (x_i = 1, if the spot is replaced and x_i = 0, if not) or continuous variables for temporal shifts (Δt_i). The regression models quantified primacy in spatial perturbations (Fig. 2G) and primacy and asymmetry for temporal perturbations (Fig. 2H). Primacy was reflected in larger-magnitude coefficients for earlier spots; temporal asymmetry was reflected in larger-magnitude coefficients for shifting spots earlier as opposed to later. Responses of individual mice are plotted in fig. S4.

The effects of temporal perturbations suggest that animals encode spot latencies referenced to sniff: As spots were shifted with respect to inhalation onset, animals' responses changed. Another possibility is that spot latencies are encoded with respect to other spots in the pattern. To test this, we considered the synchronous shift of the Target pattern, where all spots are shifted by the same amount with respect to inhalation (Fig. 3A). Synchronous shifts alter sniff-referenced timing while keeping pattern-referenced timing constant. Perceptual distances varied, but only weakly, with synchronous shifts (Fig. 3B). We attempted to predict the effect of any synchronous shift by summing the effects of single spots shifted by equal amounts referenced to inhalation. The prediction markedly overestimated the weak perceptual effect of synchronous shifts (Fig. 3B), suggesting an important role for pattern-referenced timing. Pattern-referenced timing can also be reflected in the order or sequence of spot activation. Order-changing temporal perturbations had a larger effect than order-preserving perturbations, controlling for equivalent amounts of sniff-referenced shift from the Target (Fig. 3C).

To explain the whole spectrum of behavioral results, we propose a spatiotemporal template-matching (STM) model. Template matching is the general process of comparing new inputs to

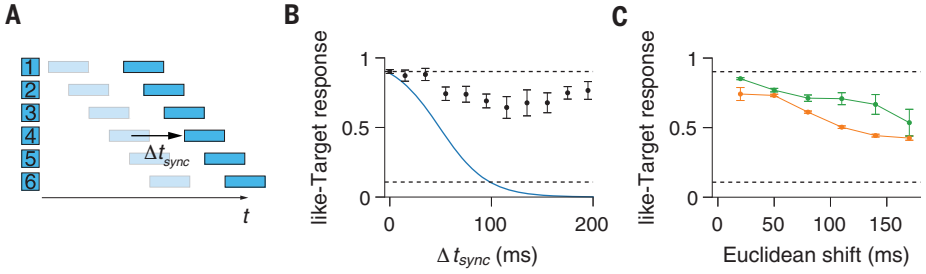

Fig. 3. Animals encode pattern-referenced timing. (**A**) Illustration of temporal perturbations in which Target patterns were shifted synchronously from inhalation by Δt_{sync}. (**B**) Like-Target response as a function of Δt_{sync} (black), with the predicted response from summing up effects of single spots shifted relative to inhalation (blue). (**C**) Comparison of average responses to temporal perturbations that preserve (green) and do not preserve (orange) temporal spot sequence for the same amount of Euclidean shift.

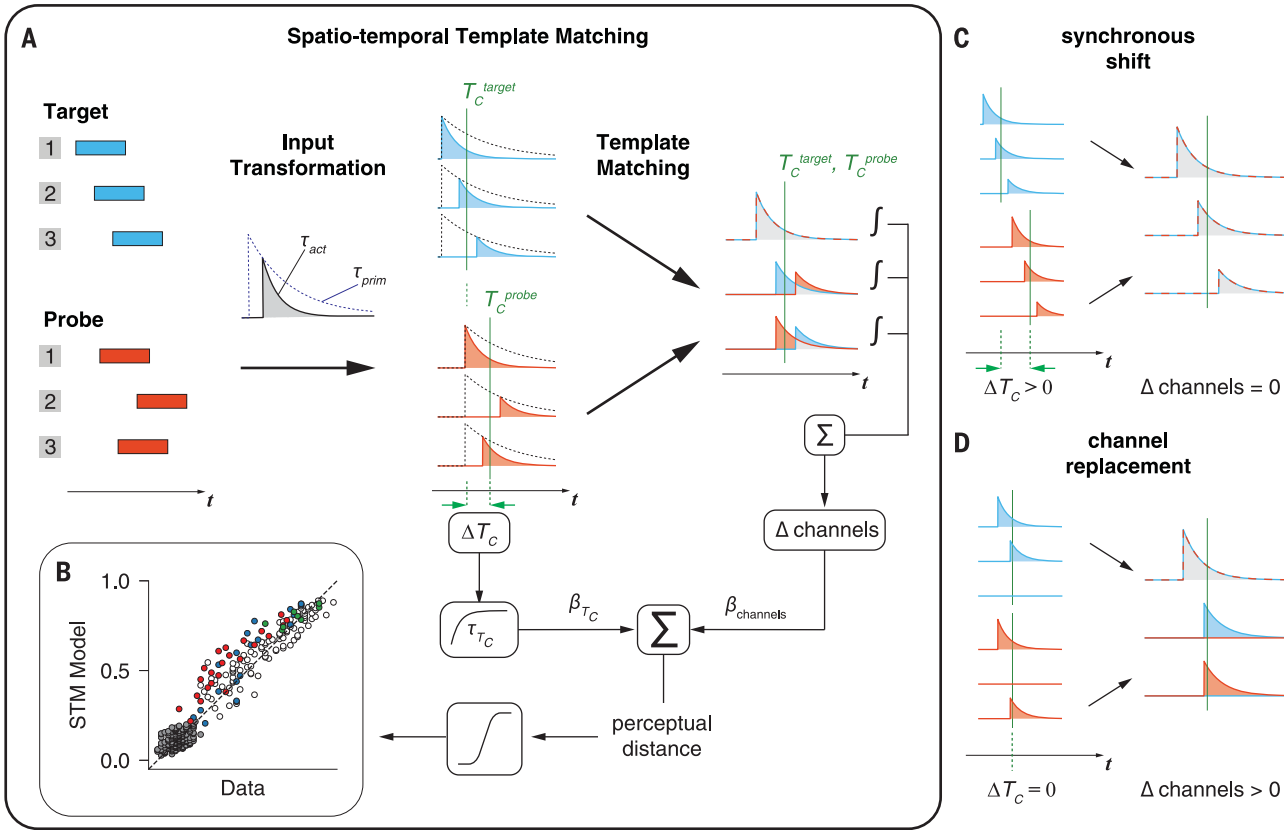

Fig. 4. STM maps olfactory inputs to perceptual outputs. (**A**) Learned pattern stored in memory (Target, blue) compared with a new input pattern (probe, red). Patterns are transformed into waveform representations: Pulse activations convolved with exponentials with decay of activation parameter τ_{act} and an amplitude that is a different exponential function (τ_{prim}) of the pulse timing from the onset of the pattern. For each set of waveforms, the center of activity, T_C^{target} and T_C^{probe}, and their absolute difference, $\Delta T_C = |T_C^{target} - T_C^{probe}|$, are calculated. Individual waveforms are then aligned to their respective pattern's center of activity and the difference in nonoverlapping area per waveform channel is integrated. This nonoverlapping area is summed linearly across all channels (Δchannels). ΔT_C is exponentiated, weighted, and then added to the weighted Δchannels value, producing a perceptual distance value. A logistic function on perceptual distances produces a probability of making a like-Target response to the given probe pattern. (**B**) STM model predictions against mouse responses across all trial types. Within each trial type, trials were sorted by perceptual distance in the model and grouped. Each dot represents a set of 50 trials. The dashed unity line indicates perfect prediction. Different colors indicate different types of perturbation: spatial, blue; synchronous temporal shifts, green; all other temporal shifts, white; Non-targets, gray; and spatial and temporal perturbation in same pattern, red. The model has the following fitting parameters: τ_{act}, τ_{prim}, τ_{T_C}, $\beta_{channels}$, β_{T_C}, and bias term β_0. (**C**) Example of template matching for synchronously shifted patterns. T_C changes, but there are no waveform differences. (**D**) Template matching for patterns in which activation in one channel is replaced by another channel. T_C does not change but waveform differences arise.

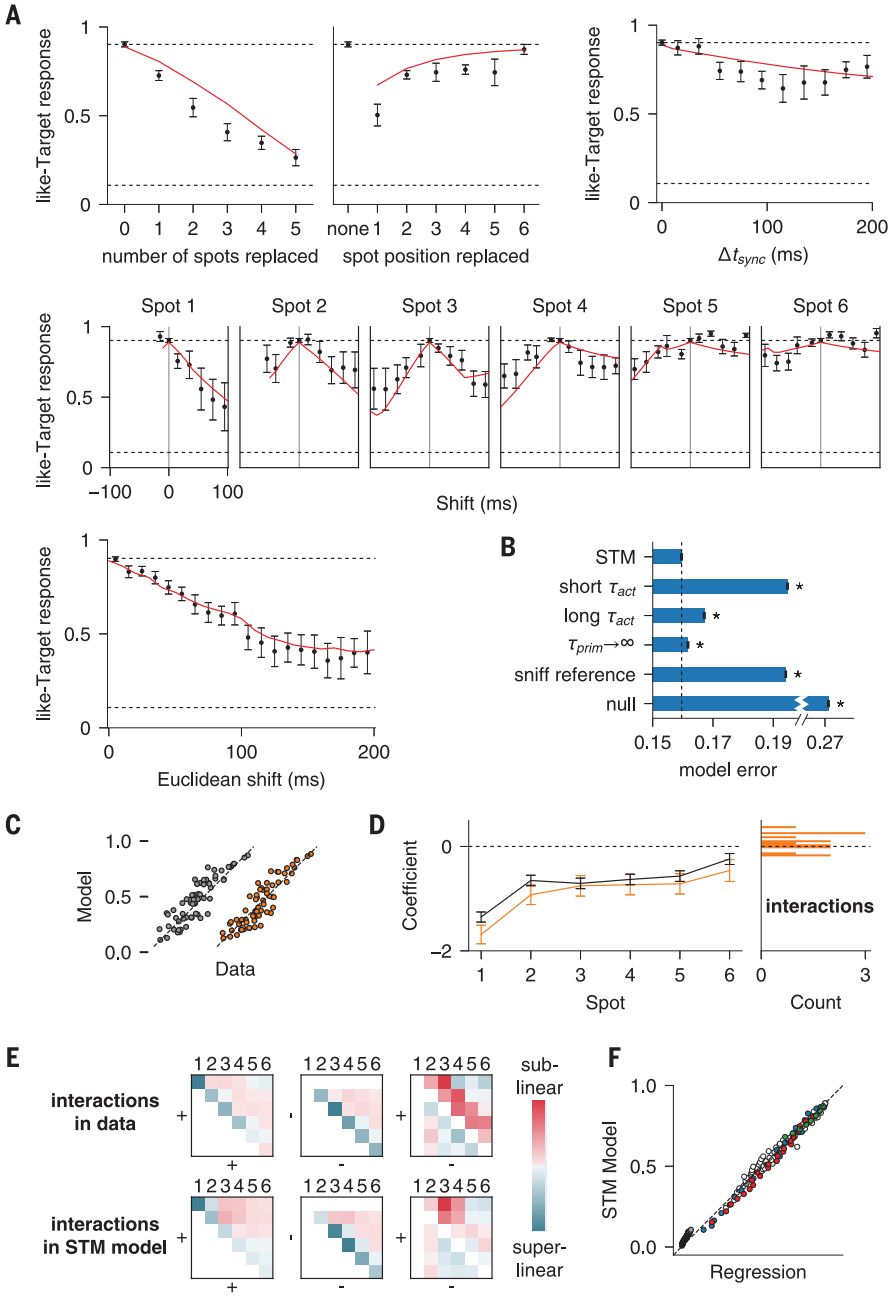

Fig. 5. Validation of the STM model. (**A**) Fits of the STM model (red) to individual spatial or temporal perturbations. (**B**) STM model compared against modified models. Vertical dashed line indicates prediction error of STM model. Short τ_{act} and long τ_{act}, changing τ_{act} from the fitted value (~60 ms) to 10 or 200 ms, respectively. $\tau_{prim} \rightarrow \infty$, setting τ_{prim} to a large value, essentially removing the primacy effect. sniff reference, within-channel comparisons referenced to sniff and not center of activity. null, null model. Asterisks indicate a $p < 0.001$ significant difference in model prediction error versus the STM model obtained from analysis of variance corrected for multiple comparisons. (**C**) Comparison of regression models for spatial perturbations, with nonlinear interactions (orange) or without (gray). The unity line (dashed) indicates perfectly predicted responses. Each dot represents a specific combination of spatial replacement by spot position. (**D**) Coefficients for models in (C) for model with interactions (orange) or without (black) plotted by spot position replaced. Right: histogram of coefficient values for interaction terms. (**E**) Comparison of temporal interactions in data as quantified by regression (top) and in simulated data run through the STM model (bottom). We considered pairwise interactions of directional shifts of spots (numbered). Left: shifting two spots later (+,+); middle: shifting two spots earlier (−,−); and right: shifting one spot later (+) and another spot earlier (−). Colors indicate magnitude and direction of interaction; red and teal indicate sublinear and superlinear interactions, meaning that the effect of paired shift is less or more than predicted from the linear sum, respectively. (**F**) Predictions of the STM model plotted against regression models for all data for the same grouping of trials as in Fig. 4B.

templates stored in memory (*26*). In systems neuroscience, template matching can refer to methods used by experimenters to compare spatiotemporal neural population activity (*27*–*29*). We propose that olfactory circuits compute similar forms of matching of neural activity for odor recognition.

The STM model consists of input transformation followed by template matching (Fig. 4A). Any olfactory input is transformed to temporal activations in discrete spatial channels (spots or, more generally, glomeruli). Activations decay over time and are represented by exponential waveforms. The decay slope reflects animals' sensitivity to temporal perturbations, with slower decays corresponding to higher invariance to temporal shifts. The strength of activations is further multiplicatively modulated by primacy, such that earlier-activated channels within the pattern evoke larger waveforms. Each learned Target input is transformed and stored as a template against which new patterns are compared.

A template-matching procedure then computes the perceptual distance between new patterns and Target templates. Template matching considers two effects independently: the difference in the center of activity and differences within individual spatial channels. The center of activity captures the average position of each template within a sniff cycle; similar centroid measures have been defined to characterize the mean response latency across multiple neurons (*30*). To perform within-channel comparisons, the model measures the amount of nonoverlap between waveforms. This comparison is done in reference to each template's center of activity. Consider synchronous shifts of Target patterns (Fig. 3B): Only the center of activity changes, not waveforms relative to the center of activity (Fig. 4C). Therefore, within-channel comparisons are primarily sensitive to changes in pattern-referenced timing as opposed to sniff-referenced timing. The choice of using a centroid model for pattern-referenced timing was further corroborated by regression analyses showing that the centroid model best predicts responses to temporal perturbations compared with other models (fig. S5). Within-channel comparisons are also sensitive to differences in spatial activations, for example, in the spot replacement of patterns (Fig. 4D). The nonoverlap per channel is then linearly summed across all channels to produce an overall channel difference value. Channel differences and the difference in center of activity are separately weighted and then combined to produce perceptual distances.

The STM model succeeded at predicting animals' responses to the whole spectrum of pattern perturbations (Fig. 4B) and reproduced the observed trends for individual perturbations (Fig. 5A). The model captured the graded effects of both spatial and temporal perturbations, with primacy in spatial perturbations

and primacy and asymmetry in temporal perturbations. The model also captured the weak effects of synchronous shifts. Changing any component in the model decreased model performance (Fig. 5B).

The STM model essentially performs a linear readout of spatial channels, because within-channel differences are summed up linearly without added interactions between channels. If animals respond to patterns according to model predictions, then the observed effects of spatial perturbations should also sum linearly. This is because replacing spots while keeping timing fixed produces only changes within channels (which are summed linearly) (Fig. 4D). We therefore compared a regression model containing only linear terms versus a regression model allowing for nonlinear effects. The nonlinear model did not perform better than the linear one (Fig. 5C, nonlinear/linear model errors = 0.160/0.158), and coefficients for nonlinear interactions were negligible (Fig. 5D).

Furthermore, a more general form of the STM model with an added parameter that allowed for possible interactions between spatial channels did not explain the data any better (see the supplementary text). Therefore, to the first approximation, the olfactory system performs a linear readout of spatial glomerular activity: Glomeruli contribute additively to the overall percept largely independently of the identity of the other activated glomeruli in the pattern.

On the other hand, the STM model predicts strong temporal interactions between channel activations: Shifting any spot changes the latencies of all other spots encoded in reference to the whole pattern. Therefore, the effect of shifting any spot depends on how other spots are shifted. We confirmed the existence of temporal interactions with regression: A regression model allowing temporal interactions between spots (Eq. 4) was superior to one that did not (model error = 0.1647 versus 0.1725, $p < 0.001$, t test). The STM model run on a large simulated dataset of random temporal perturbations produced the same pattern of temporal interactions in the data, as revealed by the regression model (Fig. 5E, $r = 0.83$).

We quantitatively compared the STM model with the best regression model fitted separately for each individual class of spatial or temporal perturbations. The regression models form a standard for comparison because they place minimal prior assumptions on the structure of the data. Despite the STM model having fewer parameters than the regressions (six versus 21), the STM model performed slightly better (model error = 0.159 versus 0.160 $p < 0.001$, t test). Furthermore, for any given pattern, the STM model and regression models produced responses that were tightly correlated (Fig. 5F), and the correlation between models was greater than the correlation between the STM model and the data ($r = 0.997$ versus $r = 0.97$). Therefore, the STM model produces patterns of responses similar to regression analyses, which could in principle capture more complex relationships within the data.

We further validated the STM model with unseen classes of spatiotemporal perturbations. In our described experiments and model fitting so far, Target pattern perturbations were either spatial or temporal, not both. We tested the fitted STM model on additional patterns containing both temporal shifts and spatial replacements within the same pattern. The model could predict animals' responses to spatiotemporal perturbations despite never encountering these manipulations during model fitting (Fig. 4B, prediction error on spatiotemporal perturbations = 0.23, spatial perturbations alone = 0.23, temporal perturbations alone = 0.21). Another form of spatiotemporal perturbations was inherent in Non-target trials, in which all Target spots were replaced and randomly shifted. No Non-target pattern was ever repeated for any animal, guaranteeing that all Non-target stimuli in model fitting were distinct from Non-target stimuli in model testing. The STM model predicted responses across different Non-targets (Fig. 4B, error = 0.10).

Our results did not merely reflect reinforcement learning of rewarded versus unrewarded stimulus (Target/Non-target) statistics, because a classifier trained to use all available reward information in the stimulation patterns did not reproduce animals' responses (fig. S6). The results also cannot be explained by animals responding idiosyncratically to probe trials (from lack of reward) because fitting the STM model to individual mice or to other groups of mice with different stimulus parameters (fig. S3) yielded similar results.

STM of olfactory bulb activity, linearly summed, constrained by activity-centered timing, and with preferential weighting on early activations, can account for how the olfactory system maps complex activity to perceptual outputs.

Discussion

We developed a framework for finding the perceptually meaningful subspace of spatiotemporal sensory activity. We optogenetically manipulated features in glomerular activity independently of other features, with manipulations that finely and extensively tiled spatiotemporal dimensions in a model-agnostic manner. By comparing all manipulations under a common metric, we derived a unifying, model-based account of olfactory computations. Other studies have used similar optogenetic techniques to probe olfaction, manipulating single-feature dimensions while measuring downstream neural responses (*11*, *17*, *31*) or the limits of behavioral discrimination (*6*, *7*, *12*). Those studies established which single-activity features are potentially accessible to the olfactory system, whereas our approach allows us to understand how features are organized in complex patterns to generate perception.

We measured how perceptual responses vary across systematic input manipulations, a basic approach in psychology applied to various classes of stimuli (e.g., images, sounds) to reveal underlying models of sensory representation (*18*, *19*). We derived models of neural representation by measuring perceptual responses across changes in neural activity.

The STM model resolves several open issues in olfactory coding. First, the model suggests a linear readout of spatial glomerular patterns. It has been proposed that odors are encoded in specific spatial combinations of glomeruli (*32*), but there are multiple possible combinatorial coding schemes that have not been tested. For example, one extreme possibility is a "barcode" representation in which any slight change to the combination leads to a completely unrelated odor, maximizing the system's representational capacity for odors. Instead, we found a perceptual readout of spatial patterns that is linear. This is consistent with studies that imaged odor-evoked glomerular activity (*33*–*35*) or directly stimulated individual glomeruli (*36*). A linear readout implies that two patterns will generate odors that are perceptually similar depending on the degree of glomerular overlap. Although a linear readout has lower representational capacity, it may explain the generalization of odor percepts across varying concentrations or backgrounds.

The role of temporal sequences in odor perception has long been hypothesized (*8*, *13*) but is not theoretically required to support odor perception (*37*). We provide direct experimental evidence for the role of temporal sequences: Mice trained to recognize a synthetic odor pattern use temporal sequences in odor recognition even though other (spatial) cues are sufficient to solve the task. These sequences were defined with relative latencies within a pattern (*10*), as opposed to latencies with respect to sniff (*6*, *8*, *13*). Pattern-referenced timing may reflect how inputs compete or are integrated downstream because competition or integration can depend on temporal proximity between inputs (*11*, *38*, *39*). Biologically plausible mechanisms for reading out these pattern-referenced sequences may involve delay circuits (*40*–*42*). Long delays on the order of 100 ms can be implemented by recurrent circuitry: In piriform cortex, recurrent excitation (*43*, *44*) or inhibition (*43*, *45*–*47*) can potentially generate sensitivity to long delays in olfactory inputs (*11*, *48*).

We found a weak perceptual effect for changing the overall position (center of activity) of the pattern within sniff, possibly arising from weak modulation of glomerular activity by sniff-coupled mechanosensory responses (*14*).

Alternatively, mice may be using the overall position of the pattern in sniff as a weak cue to solve the task, because the average randomly generated Non-target pattern has a different position within sniff compared with the Target pattern.

We found a primacy effect in which earlier-activated glomeruli had larger effects on perceptual responses. Primacy has been suggested as a strategy for animals to recognize the same odor across varying concentrations, because early-activated glomeruli remain stable across different concentrations. The ability of animals trained to recognize odors across varying concentrations was impaired during coarse optogenetic disruption, but only when the disruption occurred in the initial ~100 ms of inhalation (*15*). In the present study, animals were trained to recognize a single Target synthetic odor and displayed a primacy effect without explicit training to "concentration variants" of the Target. Therefore, the preferential weighting of early inputs occurs under different task demands, suggesting that primacy is a fundamental property of the olfactory system. Primacy may be supported by downstream computations at the level of mitral cells (*49*) or piriform cortex (*16*, *50*).

In our task, the animal could use multiple neural features to form a decision boundary for Target/Non-target discrimination because we did not tune task difficulty to the limit of perception where decision boundaries can be more confined. Therefore, we cannot rule out the possibility that nonsensory processes such as decision-making or action-related processes contributed to the observed responses, and the STM model might misattribute some of these more downstream phenomena to sensory processing alone.

We cannot rule out the possibility that fibers of passage were activated during our spot stimulation. However, this effect is likely to be weak; MT cells were activated by few localized spots at the laser intensity chosen for our experiments. Another study using similar stimulation parameters also found negligible effects of fibers of passage (*11*). Furthermore, we observed negligible nonlinear interactions between spots during spatial replacements, which would not be expected if there were widespread coactivation of glomeruli from fibers of passage.

Our experiments did not explore the dependence of perceptual similarity on the chemical tuning of glomeruli. Various studies have suggested several chemical dimensions that may correlate with perception (*51*, *52*). If perceptual similarity between glomeruli depends on chemical similarity along specific dimensions, then chemical similarity may be an additional variable that modulates interactions between glomeruli in the STM model.

Our synthetic stimuli may not capture the full complexity of glomerular activity evoked by natural odors. We view the synthetic approach as complementary to approaches using more naturalistic stimuli. The claim is not that these synthetic stimuli are direct proxies for naturalistic stimuli, but rather that synthetic stimuli afford well-controlled experiments with precise parameterization and causal manipulation, and can be used to establish basic principles of the neural code. In other well-studied sensory systems, foundational understanding of sensory processing has been built upon synthetic, reduced stimuli (*53*), whereas naturalistic stimuli have been used to test and refine foundational models (*54*).

We developed an experimental and theoretical approach that links the complex spatiotemporal language of the brain with perception and behavior. This is especially pertinent given continued advancements in optical techniques that allow direct access and manipulation of the spatiotemporal neural codes at the level of computations consequential to behavior (*55*–*58*).

Methods summary

We used OMP-ChR2 mice in which ChR2 is expressed in all olfactory glomeruli in the olfactory bulb. Dorsal olfactory bulb was exposed for optogenetic stimulation with chronically implanted glass coverslips. In separate neural recording experiments, mice were implanted with glass windows containing pre-drilled, ~1-mm holes, which allowed insertion of silicon probes for measuring mitral cell responses. For patterned optogenetic stimulation, we used digital micromirror devices in optical setups that were either purchased commercially or custom-built, allowing stimulation patterns with up to 10-μm spatial and 1-ms temporal resolution. Stimulus presentation and the recording of behavioral variables such as respiration and lick responses were performed with a custom behavioral control system based on Arduino microcontrollers. For the main behavioral experiment, mice were trained on a two-alternative forced choice task in which one lick spout was assigned to a Target pattern and the other was assigned to Non-target patterns, and mice were rewarded with a water droplet for licking to the correct spout when the associated pattern was presented. A partial reinforcement schedule was used in which only 70% of all trials were rewarded. A subset of these unrewarded trials were later substituted with probe trials (perturbations of Target patterns), such that probe trials were never rewarded regardless of the animal's response. Animals' responses on each trial were then recorded as binary responses: licking to the Target-associated spout or Non-target–associated spout. We fitted this binary response data using logistic regression models to quantify the behavioral effect along each spatial or temporal perturbation dimension. The STM model was then used to account for responses to all perturbation dimensions, both individually and combined.

REFERENCES AND NOTES

1. M. Abeles, *Corticonics: Neural Circuits of the Cerebral Cortex* (Cambridge Univ. Press, 1991).
2. G. Buzsáki, Neural syntax: Cell assemblies, synapsembles, and readers. *Neuron* **68**, 362–385 (2010). doi: 10.1016/j.neuron.2010.09.023; pmid: 21040841
3. C. A. Runyan, E. Piasini, S. Panzeri, C. D. Harvey, Distinct timescales of population coding across cortex. *Nature* **548**, 92–96 (2017). doi: 10.1038/nature23020; pmid: 28723889
4. A. R. Houweling, M. Brecht, Behavioural report of single neuron stimulation in somatosensory cortex. *Nature* **451**, 65–68 (2008). doi: 10.1038/nature06447; pmid: 18094684
5. Y. Yang, M. R. DeWeese, G. H. Otazu, A. M. Zador, Millisecond-scale differences in neural activity in auditory cortex can drive decisions. *Nat. Neurosci.* **11**, 1262–1263 (2008). doi: 10.1038/nn.2211; pmid: 18849984
6. M. Smear, R. Shusterman, R. O'Connor, T. Bozza, D. Rinberg, Perception of sniff phase in mouse olfaction. *Nature* **479**, 397–400 (2011). doi: 10.1038/nature10521; pmid: 21993623
7. M. Smear, A. Resulaj, J. Zhang, T. Bozza, D. Rinberg, Multiple perceptible signals from a single olfactory glomerulus. *Nat. Neurosci.* **16**, 1687–1691 (2013). doi: 10.1038/nn.3519; pmid: 24056698
8. R. M. Carey, J. V. Verhagen, D. W. Wesson, N. Pírez, M. Wachowiak, Temporal structure of receptor neuron input to the olfactory bulb imaged in behaving rats. *J. Neurophysiol.* **101**, 1073–1088 (2009). doi: 10.1152/jn.90902.2008; pmid: 19091924
9. H. Spors, A. Grinvald, Spatiotemporal dynamics of odor representations in the mammalian olfactory bulb. *Neuron* **34**, 301–315 (2002). doi: 10.1016/S0896-6273(02)00644-X; pmid: 11970871
10. S. Junek, E. Kludt, F. Wolf, D. Schild, Olfactory coding with patterns of response latencies. *Neuron* **67**, 872–884 (2010). doi: 10.1016/j.neuron.2010.08.005; pmid: 20826317
11. R. Haddad *et al.*, Olfactory cortical neurons read out a relative time code in the olfactory bulb. *Nat. Neurosci.* **16**, 949–957 (2013). doi: 10.1038/nn.3407; pmid: 23685720
12. M. R. Rebello *et al.*, Perception of odors linked to precise timing in the olfactory system. *PLOS Biol.* **12**, e1002021 (2014). doi: 10.1371/journal.pbio.1002021; pmid: 25514030
13. R. Shusterman, M. C. Smear, A. A. Koulakov, D. Rinberg, Precise olfactory responses tile the sniff cycle. *Nat. Neurosci.* **14**, 1039–1044 (2011). doi: 10.1038/nn.2877; pmid: 21765422
14. R. Iwata, H. Kiyonari, T. Imai, Mechanosensory-based phase coding of odor identity in the olfactory bulb. *Neuron* **96**, 1139–1152.e7 (2017). doi: 10.1016/j.neuron.2017.11.008; pmid: 29216451
15. C. D. Wilson, G. O. Serrano, A. A. Koulakov, D. Rinberg, A primacy code for odor identity. *Nat. Commun.* **8**, 1477 (2017). doi: 10.1038/s41467-017-01432-4; pmid: 29133907
16. K. A. Bolding, K. M. Franks, Recurrent cortical circuits implement concentration-invariant odor coding. *Science* **361**, eaat6904 (2018). doi: 10.1126/science.aat6904; pmid: 30213885
17. A. K. Dhawale, A. Hagiwara, U. S. Bhalla, V. N. Murthy, D. F. Albeanu, Non-redundant odor coding by sister mitral cells revealed by light addressable glomeruli in the mouse. *Nat. Neurosci.* **13**, 1404–1412 (2010). doi: 10.1038/nn.2673; pmid: 20953197
18. R. N. Shepard, Toward a universal law of generalization for psychological science. *Science* **237**, 1317–1323 (1987). doi: 10.1126/science.3629243; pmid: 3629243
19. A. Tversky, Features of similarity. *Psychol. Rev.* **84**, 327–352 (1977). doi: 10.1037/0033-295X.84.4.327
20. T. Bozza *et al.*, Mapping of class I and class II odorant receptors to glomerular domains by two distinct types of olfactory sensory neurons in the mouse. *Neuron* **61**, 220–233 (2009). doi: 10.1016/j.neuron.2008.11.010; pmid: 19186165
21. K. Mori, Y. K. Takahashi, K. M. Igarashi, M. Yamaguchi, Maps of odorant molecular features in the Mammalian olfactory bulb. *Physiol. Rev.* **86**, 409–433 (2006). doi: 10.1152/physrev.00021.2005; pmid: 16601265
22. B. A. Johnson, M. Leon, Chemotopic odorant coding in a mammalian olfactory system. *J. Comp. Neurol.* **503**, 1–34 (2007). doi: 10.1002/cne.21396; pmid: 17480025
23. L. Ma *et al.*, Distributed representation of chemical features and tunotopic organization of glomeruli in the mouse olfactory bulb. *Proc. Natl. Acad. Sci. USA.* **109**, 5481–5486 (2012). doi: 10.1073/pnas.1117491109; pmid: 22431605

24. E. R. Soucy, D. F. Albeanu, A. L. Fantana, V. N. Murthy, M. Meister, Precision and diversity in an odor map on the olfactory bulb. *Nat. Neurosci.* **12**, 210–220 (2009). doi: 10.1038/nn.2262; pmid: 19151709
25. J. Zhang, G. Huang, A. Dewan, P. Feinstein, T. Bozza, Uncoupling stimulus specificity and glomerular position in the mouse olfactory system. *Mol. Cell. Neurosci.* **51**, 79–88 (2012). doi: 10.1016/j.mcn.2012.08.006; pmid: 22926192
26. U. Neisser, in *Cognitive Psychology: Key Readings*, D. A. Balota, E. J. Marsh, Eds. (Psychology Press, 2004), pp. 125–150.
27. C. Houghton, K. Sen, A new multineuron spike train metric. *Neural Comput.* **20**, 1495–1511 (2008). doi: 10.1162/neco.2007.10-06-350; pmid: 18194108
28. A. K. Lee, M. A. Wilson, Memory of sequential experience in the hippocampus during slow wave sleep. *Neuron* **36**, 1183–1194 (2002). doi: 10.1016/S0896-6273(02)01096-6; pmid: 12495631
29. K. Louie, M. A. Wilson, Temporally structured replay of awake hippocampal ensemble activity during rapid eye movement sleep. *Neuron* **29**, 145–156 (2001). doi: 10.1016/S0896-6273(01)00186-6; pmid: 11182087
30. A. Luczak, P. Barthó, K. D. Harris, Spontaneous events outline the realm of possible sensory responses in neocortical populations. *Neuron* **62**, 413–425 (2009). doi: 10.1016/j.neuron.2009.03.014; pmid: 19447096
31. I. G. Davison, M. D. Ehlers, Neural circuit mechanisms for pattern detection and feature combination in olfactory cortex. *Neuron* **70**, 82–94 (2011). doi: 10.1016/j.neuron.2011.02.047; pmid: 21482358
32. B. Malnic, J. Hirono, T. Sato, L. B. Buck, Combinatorial receptor codes for odors. *Cell* **96**, 713–723 (1999). doi: 10.1016/S0092-8674(00)80581-4; pmid: 10089886
33. S. A. Kreher, D. Mathew, J. Kim, J. R. Carlson, Translation of sensory input into behavioral output via an olfactory system. *Neuron* **59**, 110–124 (2008). doi: 10.1016/j.neuron.2008.06.010; pmid: 18614033
34. D. Rokni, V. Hemmelder, V. Kapoor, V. N. Murthy, An olfactory cocktail party: Figure-ground segregation of odorants in rodents. *Nat. Neurosci.* **17**, 1225–1232 (2014). doi: 10.1038/nn.3775; pmid: 25086608
35. A. Mathis, D. Rokni, V. Kapoor, M. Bethge, V. N. Murthy, Reading out olfactory receptors: Feedforward circuits detect odors in mixtures without demixing. *Neuron* **91**, 1110–1123 (2016). doi: 10.1016/j.neuron.2016.08.007; pmid: 27593177
36. J. S. Bell, R. I. Wilson, Behavior reveals selective summation and max pooling among olfactory processing channels. *Neuron* **91**, 425–438 (2016). doi: 10.1016/j.neuron.2016.06.011; pmid: 27373835
37. A. Koulakov, A. Gelperin, D. Rinberg, Olfactory coding with all-or-nothing glomeruli. *J. Neurophysiol.* **98**, 3134–3142 (2007). doi: 10.1152/jn.00560.2007; pmid: 17855585
38. K. M. Franks, J. S. Isaacson, Strong single-fiber sensory inputs to olfactory cortex: Implications for olfactory coding. *Neuron* **49**, 357–363 (2006). doi: 10.1016/j.neuron.2005.12.026; pmid: 16446140
39. A. Apicella, Q. Yuan, M. Scanziani, J. S. Isaacson, Pyramidal cells in piriform cortex receive convergent input from distinct olfactory bulb glomeruli. *J. Neurosci.* **30**, 14255–14260 (2010). doi: 10.1523/JNEUROSCI.2747-10.2010; pmid: 20962246
40. J. J. Hopfield, Pattern recognition computation using action potential timing for stimulus representation. *Nature* **376**, 33–36 (1995). doi: 10.1038/376033a0; pmid: 7596429
41. H. Sanders *et al*., A network that performs brute-force conversion of a temporal sequence to a spatial pattern: Relevance to odor recognition. *Front. Comput. Neurosci.* **8**, 108 (2014). doi: 10.3389/fncom.2014.00108; pmid: 25278870
42. D. W. Tank, J. J. Hopfield, Neural computation by concentrating information in time. *Proc. Natl. Acad. Sci, USA.* **84**, 1896–1900 (1987). doi: 10.1073/pnas.84.7.1896; pmid: 3470765
43. K. M. Franks *et al*., Recurrent circuitry dynamically shapes the activation of piriform cortex. *Neuron* **72**, 49–56 (2011). doi: 10.1016/j.neuron.2011.08.020; pmid: 21982368
44. C. Poo, J. S. Isaacson, A major role for intracortical circuits in the strength and tuning of odor-evoked excitation in olfactory cortex. *Neuron* **72**, 41–48 (2011). doi: 10.1016/j.neuron.2011.08.015; pmid: 21982367
45. M. Satou, K. Mori, Y. Tazawa, S. F. Takagi, Interneurons mediating fast postsynaptic inhibition in pyriform cortex of the rabbit. *J. Neurophysiol.* **50**, 89–101 (1983). doi: 10.1152/jn.1983.50.1.89; pmid: 6875654
46. C. C. A. Stokes, J. S. Isaacson, From dendrite to soma: Dynamic routing of inhibition by complementary interneuron microcircuits in olfactory cortex. *Neuron* **67**, 452–465 (2010). doi: 10.1016/j.neuron.2010.06.029; pmid: 20696382
47. N. Suzuki, J. M. Bekkers, Microcircuits mediating feedforward and feedback synaptic inhibition in the piriform cortex. *J. Neurosci.* **32**, 919–931 (2012). doi: 10.1523/JNEUROSCI.4112-11.2012; pmid: 22262890
48. L. B. Haberly, Summed potentials evoked in opossum prepyriform cortex. *J. Neurophysiol.* **36**, 775–788 (1973). doi: 10.1152/jn.1973.36.4.775; pmid: 4713319
49. E. M. Arneodo *et al*., Stimulus dependent diversity and stereotypy in the output of an olfactory functional unit. *Nat. Commun.* **9**, 1347 (2018). doi: 10.1038/s41467-018-03837-1; pmid: 29632302
50. K. A. Bolding, K. M. Franks, Complementary codes for odor identity and intensity in olfactory cortex. *eLife* **6**, e22630 (2017). doi: 10.7554/eLife.22630; pmid: 28379135
51. A. Keller *et al*., Predicting human olfactory perception from chemical features of odor molecules. *Science* **355**, 820–826 (2017). doi: 10.1126/science.aal2014; pmid: 28219971
52. K. Snitz *et al*., Predicting odor perceptual similarity from odor structure. *PLOS Comput. Biol.* **9**, e1003184 (2013). doi: 10.1371/journal.pcbi.1003184; pmid: 24068899
53. D. H. Hubel, T. N. Wiesel, Receptive fields of single neurones in the cat's striate cortex. *J. Physiol.* **148**, 574–591 (1959). doi: 10.1113/jphysiol.1959.sp006308; pmid: 14403679
54. N. C. Rust, J. A. Movshon, In praise of artifice. *Nat. Neurosci.* **8**, 1647–1650 (2005). doi: 10.1038/nn1606; pmid: 16306892
55. G. M. Lerman, J. V. Gill, D. Rinberg, S. Shoham, Precise optical probing of perceptual detection. bioRxiv 456764 [Preprint] 30 October 2018; https://doi.org/10.1101/456764.
56. A. M. Packer, L. E. Russell, H. W. P. Dalgleish, M. Häusser, Simultaneous all-optical manipulation and recording of neural circuit activity with cellular resolution in vivo. *Nat. Methods* **12**, 140–146 (2015). doi: 10.1038/nmeth.3217; pmid: 25532138
57. L. Carrillo-Reid, S. Han, W. Yang, A. Akrouh, R. Yuste, Controlling visually guided behavior by holographic recalling of cortical ensembles. *Cell* **178**, 447–457.e5 (2019). doi: 10.1016/j.cell.2019.05.045; pmid: 31257030
58. J. H. Marshel *et al*., Cortical layer-specific critical dynamics triggering perception. *Science* **365**, eaaw5202 (2019). doi: 10.1126/science.aaw5202; pmid: 31320556
59. E. Chong, M. Moroni, C. Wilson, S. Shoham, S. Panzeri, D. Rinberg, Code for: Manipulating synthetic optogenetic odors reveals the coding logic of olfactory perception, Zenodo (2020); https://doi.org/10.5281/zenodo.3698314.

ACKNOWLEDGMENTS

We thank A. Resulaj, G. Serrano, A. Pickens, S. Stark, S. Toole, H. Ma, G. Lerman, J. Kappel, N. Amin, A. Oganov, M. Robles-Long, and A. Pillai for assistance in building and running experiments and B. Mensh, K. Nagel, T. Movshon, W. Ma, J. Gill, and H. Nakayama for helpful comments. **Funding:** This work was supported by NIH BRAIN Initiative Grants R01NS109961 to D.R. and S.P. and U19NS107464 to D.R., S.P., and S.S. **Author contributions:** E.C., S.P., S.S., and D.R. conceived and designed the experimental, computational, and modeling approaches; E.C. and C.W. built the experimental system and performed experiments; M.M., C.W., and E.C. performed computational analyses; E.C., M.M., S.S., S.P., and D.R. wrote the manuscript; and S.P. and D.R. supervised the project. **Competing interests:** The authors declare no competing interests. **Data and materials availability:** Datasets and analysis code will be available at Zenodo (*59*).

SUPPLEMENTARY MATERIALS

science.sciencemag.org/content/368/6497/eaba2357/suppl/DC1
Materials and Methods
Supplementary Text
Figs. S1 to S7
References (*60*–*66*)

View/request a protocol for this paper from *Bio-protocol*.

15 November 2019; accepted 1 May 2020
10.1126/science.aba2357